© 2018. Published by The Company of Biologists Ltd | Biology Open (2018) 7, bio031799. doi:10.1242/bio.031799

RESEARCH ARTICLE

Functional comparison of distinct *Brachyury*$^+$ states in a renal differentiation assay

Jing Zhou, Antonius Plagge and Patricia Murray*

ABSTRACT

Mesodermal populations can be generated *in vitro* from mouse embryonic stem cells (mESCs) using three-dimensional (3-D) aggregates called embryoid bodies or two-dimensional (2-D) monolayer culture systems. Here, we investigated whether *Brachyury*-expressing mesodermal cells generated using 3-D or 2-D culture systems are equivalent or, instead, have different properties. Using a *Brachyury*-GFP/E2-Crimson reporter mESC line, we isolated *Brachyury*-GFP$^+$ mesoderm cells using flow-activated cell sorting and compared their gene expression profiles and *ex vivo* differentiation patterns. Quantitative real-time polymerase chain reaction analysis showed significant up-regulation of *Cdx2*, *Foxf1* and *Hoxb1* in the *Brachyury*-GFP$^+$ cells isolated from the 3-D system compared with those isolated from the 2-D system. Furthermore, using an *ex vivo* mouse kidney rudiment assay, we found that, irrespective of their source, *Brachyury*-GFP$^+$ cells failed to integrate into developing nephrons, which are derived from the intermediate mesoderm. However, *Brachyury*-GFP$^+$ cells isolated under 3-D conditions appeared to differentiate into endothelial-like cells within the kidney rudiments, whereas the *Brachyury*-GFP$^+$ isolated from the 2-D conditions only did so to a limited degree. The high expression of *Foxf1* in the 3-D *Brachyury*-GFP$^+$ cells combined with their tendency to differentiate into endothelial-like cells suggests that these mesodermal cells may represent lateral plate mesoderm.

KEY WORDS: Mouse embryonic stem cells, Embryoid bodies, *Brachyury*, Mesodermal differentiation, *Ex vivo* culture, Kidney rudiments

INTRODUCTION

The formation of the primitive streak (PS) marks the onset of antero-posterior axis determination in the developing mouse embryo (Stern, 2004; Rodriguez et al., 2005). The epiblast cells egress through the PS to generate the nascent mesoderm in between the primitive ectoderm and the overlying visceral endoderm. *Brachyury* (*Bra*, also known as *T*) is the key marker of the entire PS and is a pan mesodermal marker that is expressed in the posterior epiblast, PS, node, notochord, allantois and tail bud (Wilkinson et al., 1990; Kispert and Herrmann, 1994; Conlon et al., 1995; Kispert et al., 1995; King et al., 1998; Showell et al., 2004; Papaioannou, 2014; Concepcion and Papaioannou, 2014).

Following gastrulation, the *Bra*$^+$ nascent mesoderm generates (i) paraxial mesoderm, which gives rise to the somites; (ii) lateral plate mesoderm, which gives rise to the heart, vessels, haematopoietic stem cells and endothelial cells; and (iii) intermediate mesoderm, which gives rise to the urogenital system (Gilbert, 2010; Wolpert et al., 2015). The intermediate mesoderm then becomes further specified to anterior intermediate mesoderm that gives rise to the ureteric bud (UB), and posterior intermediate mesoderm that gives rise to the metanephric mesenchyme (MM) (Little et al., 2016). The UB and MM generate the collecting ducts and nephrons, respectively, of the mature kidney (Pietilä and Vainio, 2014; Little et al., 2016).

The small size and inaccessibility of the peri-implantation mouse embryo makes it difficult to study. However, the isolation of embryonic stem cells (ESCs) from mouse blastocysts in the 1980s (Evans and Kaufman, 1981; Martin, 1981) has provided an alternative model for studying the early development of the mouse embryo.

When cultured in suspension, mouse ESCs (mESCs) spontaneously form spheroid multicellular aggregates called embryoid bodies (EBs) (Wobus et al., 1984; Doetschman et al., 1985; Robertson, 1987; Murray and Edgar, 2000, 2004). A typical EB has an outer layer of primitive endoderm, an inner layer of primitive ectoderm, a basement membrane separating them, as well as a central cavity that resembles the proamniotic cavity (Shen and Leder, 1992). The primitive ectoderm differentiates to generate derivatives of definitive ectoderm, endoderm and mesoderm (Wobus et al., 1984; Doetschman et al., 1985; Keller et al., 1993). Therefore, EBs can recapitulate some aspects of peri-implantation mouse development and provide an excellent model system for studying these early events (Wobus et al., 1984; Doetschman et al., 1985; Robertson, 1987).

However, the heterogeneous nature of the EBs means that the extent of differentiation towards any specific cell type can vary considerably depending on culture conditions, and can even vary between EBs cultured under the same culture conditions. The complex three-dimensional (3-D) structure also hinders the visualisation of the differentiation process at an individual cell level. For this reason, various two-dimensional (2-D) differentiation protocols have been developed to direct differentiation to specific cell types more efficiently. Several studies have demonstrated *in vitro* derivation of monolayer mESCs into lineages of neural progenitors, endothelial cells, osteochondrogenic and myogenic cells using chemically defined media (Ying and Smith, 2003; Sakurai et al., 2009; Blancas et al., 2011, 2013). Recently, Turner et al. showed that *Activin/Nodal* and *Wnt* signalling pathways promote mesoderm formation in monolayer mESC culture, with the mesodermal cells differentiated from mESCs displaying *Bra* expression, similarly to the nascent mesoderm that develops in the primitive streak of developing mouse embryos and of 'gastrulating'

Department of Cellular and Molecular Physiology, Institute of Translational Medicine, University of Liverpool, Liverpool L69 3BX, UK.

*Author for correspondence (P.A.Murray@liverpool.ac.uk)

J.Z., 0000-0003-1974-9946; P.M., 0000-0003-1316-148X

Received 20 December 2017; Accepted 9 April 2018

Biology Open (2018) 7, bio031799. doi:10.1242/bio.031799

EBs (Turner et al., 2014a,b). By using a combination of Activin A (*Activin/Nodal* agonist) and Chiron (*Wnt3a* agonist), this group developed a highly efficient strategy for inducing E14 mESCs to differentiate into nascent mesoderm.

Although mesoderm differentiation occurs within both the 3-D EB and 2-D mESC culture systems, it is not clear whether the differentiated cells (e.g. mesodermal cells) that are generated by the 2-D protocols are equivalent to those that form in EBs. In the mouse embryo, the fate of the *Bra*$^+$ cells is determined by the microenvironment that the cells find themselves in following their migration from the primitive streak (Gilbert, 2010). This cannot be replicated using *in vitro* culture systems, which raises the question of whether the *Bra*$^+$ cells generated *in vitro* are equivalent to nascent mesoderm or, instead, are partially committed to a specific mesodermal lineage. For instance, Takasato et al. previously reported that BRA$^+$ cells derived from human ESCs have a tendency to spontaneously differentiate into FOXF1$^+$ lateral plate mesoderm when cultured in the absence of exogenous growth factors (Takasato et al., 2014). This observation highlights the fact that the differentiation potential of *Bra*$^+$ cells generated *in vitro* is likely to be influenced by the specific culture conditions used.

We have previously shown that *Bra*$^+$ mesodermal cells isolated from mESC-derived EBs were able to integrate into the developing UB and MM of mouse kidney rudiments and generate specialised renal cells (Rak-Raszewska et al., 2012). However, in this previous study, the EBs from which the *Bra*$^+$ mesodermal cells were isolated did not mimic early embryo development, in that they did not form a primitive ectoderm epithelium, nor a proamniotic cavity. In the present study, we aimed to investigate whether *Bra*$^+$ cells generated using the recently described 2-D culture system, and those derived from cavitating EBs, express similar lineage-specific genes, and have similar developmental potential to those derived from non-cavitating EBs. In order to do this, we have generated a *Bra-GFP/Rosa26-E2C* mESC reporter line (Zhou et al., 2018) that will allow us to isolate the GFP-expressing mesodermal cells from both systems so that their gene expression can be analysed using RT-PCR and their developmental potential can be assessed by investigating their fate following incorporation into mouse kidney rudiments *ex vivo* (Unbekandt and Davies, 2010; Kuzma-Kuzniarska et al., 2012; Rak-Raszewska et al., 2012; Ranghini et al., 2013; Dauleh et al., 2016).

RESULTS

Mesoderm development within EBs is affected by seeding density

The *Bra-GFP/Rosa26-E2C* mESCs were seeded at different densities and cultivated for 7 days in EB medium. At densities of 2.5×10^5 and 1.25×10^5 cells ml^{-1}, cavitated EBs could be observed by day 4, but at the lower seeding density of 6.25×10^4 cells ml^{-1}, most EBs failed to cavitate, even by day 7 (Fig. 1; Fig. S1). Mesoderm development was identified in all conditions by GFP fluorescence, but the expression patterns were different. At 6.25×10^4 cells ml^{-1}, GFP was expressed at an earlier stage and peaked on day 4 before decreasing. In contrast, at higher densities, GFP became visible at day 4 or later and the fluorescence signal increased from day 4 to 7, but there appeared to be more GFP$^+$ cells in the 1.25×10^5 cells ml^{-1} EBs (Fig. 1A). Therefore, given that the EBs developing in the 1.25×10^5 cells ml^{-1} density cultures appeared to be typical cavitating EBs that contained a high proportion of GFP$^+$ cells, we used this plating density in all future experiments. To investigate if E2C expression affected mesoderm differentiation, immunostaining of *Bra-GFP/Rosa26-E2C* EB sections was performed to confirm that the GFP$^+$ cells within the EB expressed E2C. The results showed that all cells within the *Bra-GFP/Rosa26-E2C* EBs continued to express E2C, including the GFP$^+$ mesodermal cells, indicating that E2C expression did not inhibit mesoderm differentiation (Fig. 1B).

Comparing the timing and extent of mesodermal cell differentiation using the 3-D and 2-D culture systems

In order to accurately monitor changes in GFP expression in the developing EBs over time, *Bra-GFP/Rosa26-E2C* mESCs were plated at a density of 1.25×10^5 cells ml^{-1}, and at day 3 were embedded in a sandwich-like agarose system (2% agarose bottom layer – EB – 1% agarose overlay) and imaged in real-time using the Cell-IQ instrument every hour from day 5 to day 8 post-plating (Movie 1). GFP started to be expressed on day 5 (132 h), and reached maximum levels on day 6–7 (Fig. 2A). To quantify the proportion of mesodermal cells within the EBs, flow cytometry analysis was performed. EBs derived from the wild-type E14TG2a mESCs were used as a negative control. The results were comparable to the Cell-IQ data, and showed that the peak GFP expression was at day 6, at which time, ∼39% of the EB population was GFP$^+$ (Fig. 2B).

We then determined the efficiency of the previously described 2-D culture system (Turner et al., 2014a,b). The *Bra-GFP/Rosa26-E2C* mESCs were cultured under differentiation conditions for 4 days, and were then screened for GFP expression. The 4-day time point was chosen because it has been indicated in a previous publication that the GFP expression peaks at day 4 using this differentiation protocol (Turner et al., 2014b). Analysis of fixed cells in culture showed that the vast majority of the population expressed GFP. Flow cytometry analysis showed that ∼89% of the population was GFP$^+$, which is consistent with the efficiency reported previously with this method (Fig. 2C,D).

Comparing the expression profile of key genes in GFP$^+$ mesodermal cells generated under 3-D and 2-D differentiation conditions

Before comparing the expression levels of the key target genes in the GFP$^+$ cells isolated from the 3-D and 2-D culture systems, it was first necessary to determine the purity of the GFP$^+$ cell populations isolated from each culture system. Single-cell suspensions from day 6 EBs and day 4 2-D monolayer cultures were sorted by fluorescence-activated cell sorting (FACS) and then re-analysed using the same parameters. Results showed that the proportion of GFP$^+$ cells was over 94% (Fig. 3A), confirming they were pure populations.

In order to characterise the *Bra*-GFP$^+$ and *Bra*-GFP$^-$ populations, quantitative real-time polymerase chain reaction (qRT-PCR) was performed to examine the expression patterns of key genes of mesodermal lineages and of early kidney development (Table S1) (Erselius et al., 1990; Herrmann et al., 1990; Lin et al., 1993; Sánchez et al., 1996; Kmita et al., 2000; Chapman et al., 2003; Carapuço et al., 2005; Basson et al., 2006; Gadue et al., 2006; Arnold and Robertson, 2009; Dressler, 2009; Savory et al., 2009; Yallowitz et al., 2011; Little, 2015). Relative gene expression levels were evaluated and compared between the following groups: (i) the *Bra*-GFP$^+$ and *Bra*-GFP$^-$ populations isolated from the EBs (3-D system); (ii) the *Bra*-GFP$^+$ and *Bra*-GFP$^-$ populations isolated from the 2-D system; and (iii) the *Bra*-GFP$^+$ populations isolated from the 3-D and 2-D systems. Stemness markers *Oct4* and *Nanog* and the primitive ectoderm marker, *Fgf5*, were also evaluated to assess whether undifferentiated mESCs and/or ectoderm cells were present.

Biology Open (2018) 7, bio031799. doi:10.1242/bio.031799

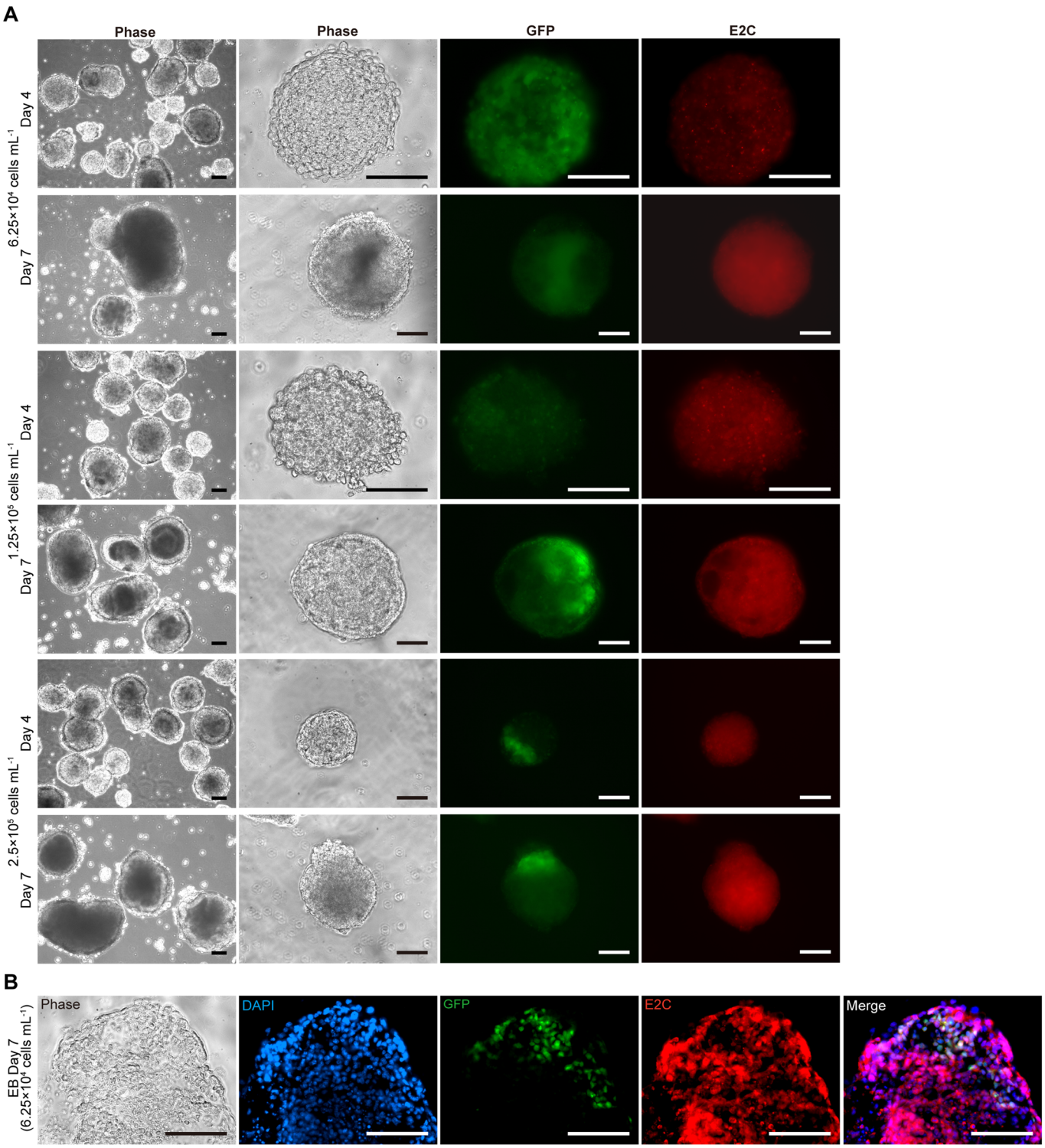

Fig. 1. Representative fluorescence and phase-contrast photomicrographs of mesoderm development within EBs derived from *Bra-GFP*/*Rosa26-E2C* mESCs at different seeding densities cultured for up to 7 days. (A) EB morphology was examined on days 4 and 7. The majority of EBs derived from mESCs plated at densities of 2.5×10^5 and 1.25×10^5 cells ml^{-1} showed evidence of cavitation, whereas cavitated EBs were less abundant in the lower density culture (6.25×10^4 cells ml^{-1}). Maximal levels of GFP expression were observed in day 7 EBs derived from the 1.25×10^5 density cultures. (B) Immunostaining of cryo-sections of day 7 EBs for E2C, counterstained with DAPI. Representative photomicrographs of lower density culture showed that all cells within the EBs derived from the E2C-expressing mESCs stained positively for E2C (red), including the GFP^+ (green) mesodermal cells. Data were collected from three biological replicates. Scale bars: 100 µm.

Firstly, comparisons were made between gene expression levels in the *Bra*-GFP^+ cells and the *Bra*-GFP^- cells isolated from the 3-D and 2-D system. The results showed that the early mesoderm genes *Bra*, *Cdx2*, *Tbx6*, *Foxf1*, *Foxa2*, *Hoxb1* and *Hoxc9* were expressed by *Bra*-GFP^+ cells isolated from both the 3-D and 2-D systems, but the relative expression levels differed in comparison to the

Biology Open (2018) 7, bio031799. doi:10.1242/bio.031799

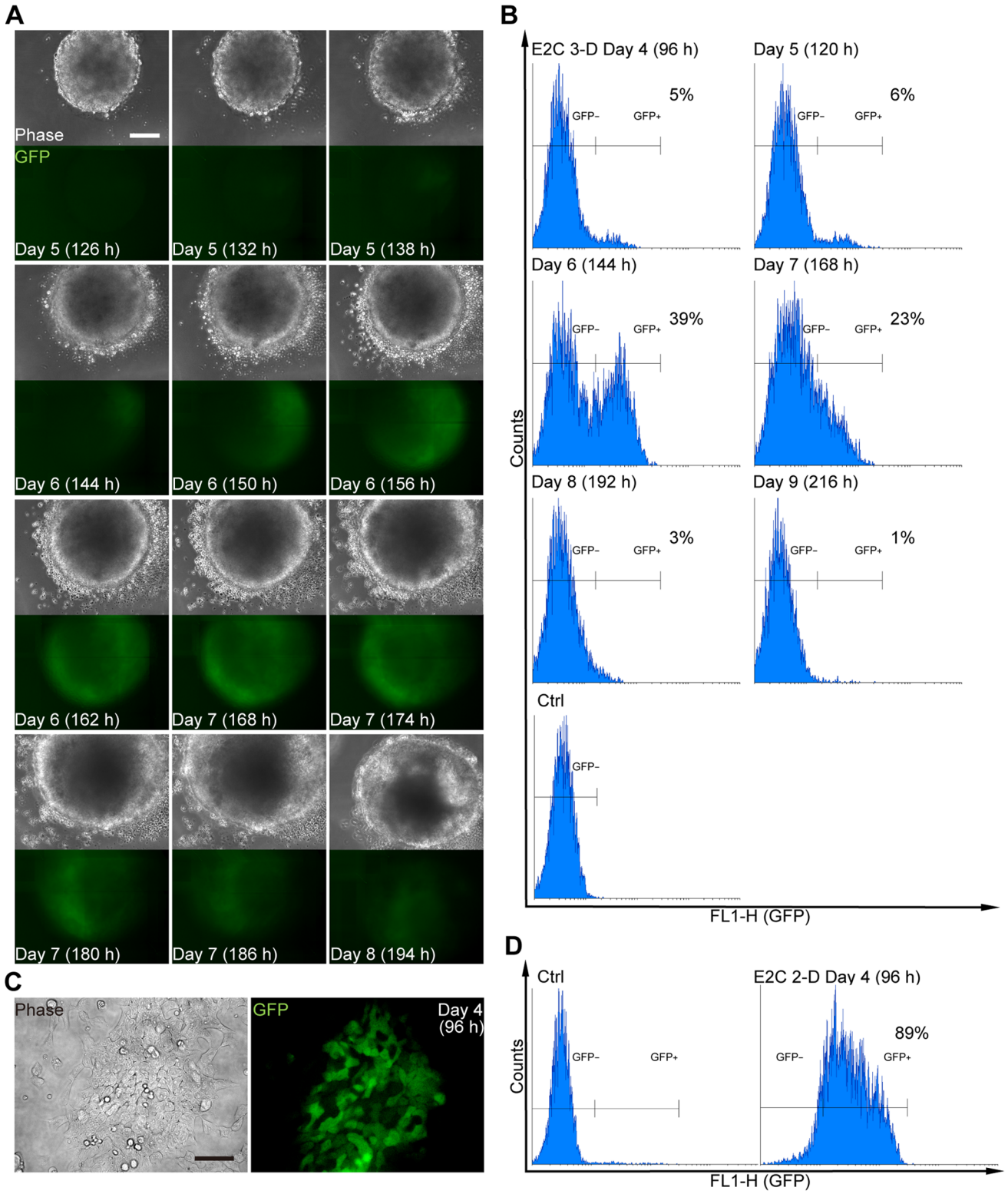

Fig. 2. Timing and extent of GFP expression in *Bra-GFP*/*Rosa26-E2C* mESCs following mesodermal differentiation in 3-D and 2-D culture systems. (A) Fluorescence and phase contrast photomicrographs of EBs derived from mESCs seeded at 1.25×10^5 cells ml^{-1}. EBs were cultured for up to 9 days and imaged in real-time every hour from day 5 to day 8 post-plating. (B) Flow cytometry analysis of disaggregated *Bra-GFP*/*Rosa26-E2C* EBs at different time points revealed that GFP started to be expressed on day 4, and reached maximum levels on days 6–7. At the peak of expression (day 6), GFP^+ cells comprised 39% of the population. (C) Representative fluorescence and phase-contrast photomicrographs of mESCs following directed differentiation to mesoderm using a 2-D culture system. Four days following induction, cells no longer formed colonies, appeared differentiated, and the majority expressed GFP. (D) Flow cytometry analysis showed that ∼89% of cells expressed GFP under 2-D culture conditions. Undifferentiated *Bra-GFP*/*Rosa26-E2C* mESCs sub-cultured in gelatinised dishes in mESC medium for 24 h prior to induction were used as a negative control. Data were collected from at least two biological replicates. Scale bars: 200 µm (A); 100 µm (C).

Biology Open (2018) 7, bio031799. doi:10.1242/bio.031799

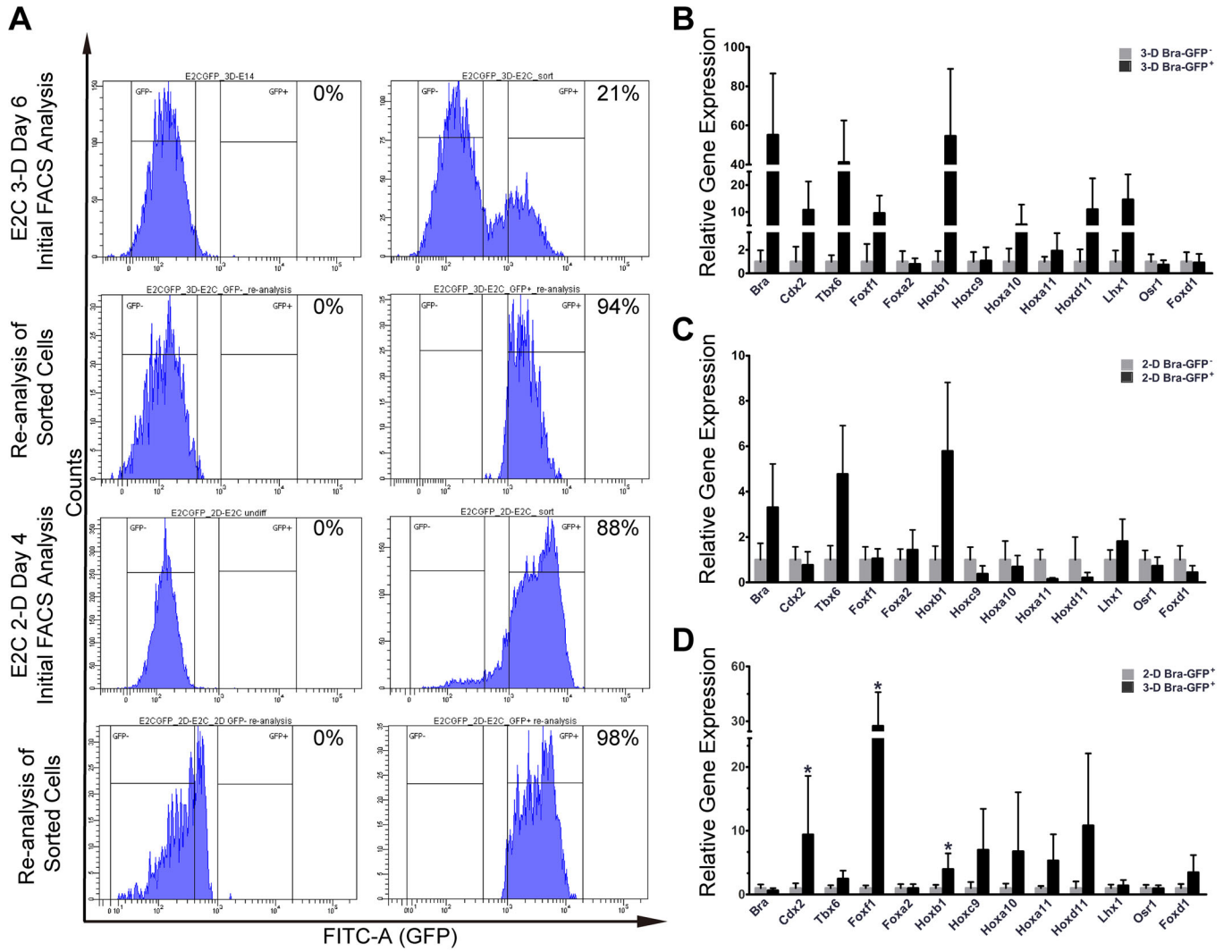

Fig. 3. Isolation and analysis of gene expression profiles of the mesodermal and non-mesodermal populations from *Bra-GFP*/*Rosa26-E2C* mESCs cultured in 3-D and 2-D systems. (A) Day 6 EBs or mESCs cultured under 2-D differentiating conditions for 4 days were harvested for FACS. Untransfected day 6 *E14-Bra-GFP* EBs or mESCs maintained undifferentiated in gelatinised dishes in mESC medium for 24 h prior to induction were used as negative controls. Flow cytometry was used to confirm the purity of the populations isolated using FACS. (B) Relative expression levels of mesoderm and early kidney development genes were compared between *Bra*-GFP$^+$ and *Bra*-GFP$^-$ populations isolated from the 3-D system (n=2 biological replicates), presented as mean±s.e.m. Data were not statistically assessed on significance due to there being two biological replicates; however, they gave an indication of the difference between *Bra*-GFP$^+$ and *Bra*-GFP$^-$ populations. (C) Relative expression levels of mesoderm and early kidney development genes were compared between *Bra*-GFP$^+$ and *Bra*-GFP$^-$ populations isolated from the 2-D system (n=2 biological replicates), presented as mean±s.e.m. Data were not statistically assessed on significance due to there being two biological replicates; however, they gave an indication of the difference between *Bra*-GFP$^+$ and *Bra*-GFP$^-$ populations. (D) Relative gene expression levels of mesoderm and early kidney development genes were compared between *Bra*-GFP$^+$ populations isolated from 3-D system (n=3 biological replicates) and 2-D system (n=3 biological replicates), presented as mean±s.e.m. *P<0.05 was considered statistically significant (t-test).

respective *Bra*-GFP$^-$ populations. For instance, under the 3-D conditions, the expression levels of *Bra*, *Cdx2*, *Tbx6*, *Foxf1*, and *Hoxb1* in the *Bra*-GFP$^+$ population were ∼55-, 10-, 40-, 10- and 55-fold higher than in the *Bra*-GFP$^-$ population, respectively, whereas under the 2-D conditions, *Bra*, *Tbx6* and *Hoxb1* levels in the *Bra*-GFP$^+$ cells were only 2-, 4-, and 5-fold higher, respectively, than in the *Bra*-GFP$^-$ cells (Fig. 3B,C).

There was a 1- to 10-fold up-regulation of Hox10 and Hox11 paralogy groups (*Hoxa10*, *Hoxa11* and *Hoxd11*) in the *Bra*-GFP$^+$ population compared to the *Bra*-GFP$^-$ population isolated from cells under 3-D conditions. In contrast, down-regulation of the same genes was observed in the *Bra*-GFP$^+$ population isolated from cells under 2-D conditions compared to the *Bra*-GFP$^-$ population (Fig. 3B,C). This suggested that the status of *Bra*-GFP$^+$ cells isolated from EBs may be closer to a stage resembling posterior mesoderm, as it has been shown previously that posterior mesoderm, which gives rise to the MM, expresses higher levels of *Hox10* and *11* genes compared to anterior mesoderm (Taguchi et al., 2014).

Genes of intermediate mesoderm and metanephric mesenchyme, i.e. *Lhx1*, *Osr1*, *Pax2* and *Wt1*, displayed a similar trend in the change of relative expression levels between the *Bra*-GFP$^+$ and *Bra*-GFP$^-$ groups under 3-D and 2-D conditions. It is of note that in the cells isolated from the EBs, *Lhx1* was up-regulated by ∼10-fold in the *Bra*-GFP$^+$ cells compared to the *Bra*-GFP$^-$ cells, whereas there was minimal up-regulation in the *Bra*-GFP$^+$ cells isolated from

Biology Open (2018) 7, bio031799. doi:10.1242/bio.031799

the 2-D conditions (Fig. 3B,C; Fig. S2). *Oct4*, *Nanog* and *Fgf5* were also evaluated and the data showed no difference between the *Bra*-GFP$^+$ cells and *Bra*-GFP$^-$ cells isolated from both 3-D and 2-D conditions (Fig. S2).

Next, the relative expression levels of the various genes in *Bra*-GFP$^+$ cells isolated from 3-D and 2-D system was compared. There was no significant difference in the expression levels of *Bra* and *Tbx6*, whereas *Cdx2*, *Foxf1* and *Hoxb1* were significantly up-regulated by 9-, 30-, 5-fold, respectively, in the *Bra*-GFP$^+$ cells isolated under 3-D conditions. Another early mesoderm gene, *Hoxc9*, as well as posterior mesoderm genes *Hox10* and *Hox11*, were also up-regulated but not significantly. The expression levels of *Lhx1*, *Osr1*, *Pax2*, *Wt1* and *Gdnf* were comparable between the two populations. On the other hand, *Foxd1*, which, is expressed in MM and stroma, showed a slight 2-fold up-regulation in the 3-D *Bra*-GFP$^+$ cells, but this was not statistically significant (Fig. 3D; Fig. S2).

Ex vivo development of intact and re-aggregated non-chimeric mouse kidney rudiments

In order to evaluate how the *Bra*-GFP$^+$ cells behave in the rudiment culture, it was first necessary to establish the typical staining pattern of various renal cell-specific antibodies in intact kidney rudiments cultured *ex vivo*. Following 5 days of *ex vivo* culture, the rudiments were fixed and immunofluorescence was performed to detect the following markers: megalin, which is expressed on the apical surfaces of proximal tubule cells (Ranghini et al., 2013; Taguchi et al., 2014); Wt1, which is expressed in MM and developing nephrons, and expressed at very high levels in nascent and mature podocytes (Moore et al., 1999; Ranghini et al., 2013; Taguchi et al., 2014); and synaptopodin, which is expressed in mature podocytes (Mundel et al., 1997; Shankland et al., 2007). The rudiments were also stained with rhodamine-labelled peanut agglutinin (PNA), which mainly binds to the basement membranes of UBs, and more weakly to those of the developing nephrons (Laitinen et al., 1987). PNA staining showed an intact UB tree, and immunostaining for megalin showed typical staining of the apical surfaces of proximal tubule cells (Fig. 4A). As expected, immunostaining for Wt1 showed weaker expression in MM and developing nephrons and intense expression in nascent and mature podocytes, whereas synaptopodin was exclusively expressed in mature podocytes (Fig. 4A).

To confirm that re-aggregated kidney rudiments could develop nephron and UB structures as previously reported (Unbekandt and Davies, 2010; Rak-Raszewska et al., 2012; Ranghini et al., 2013),

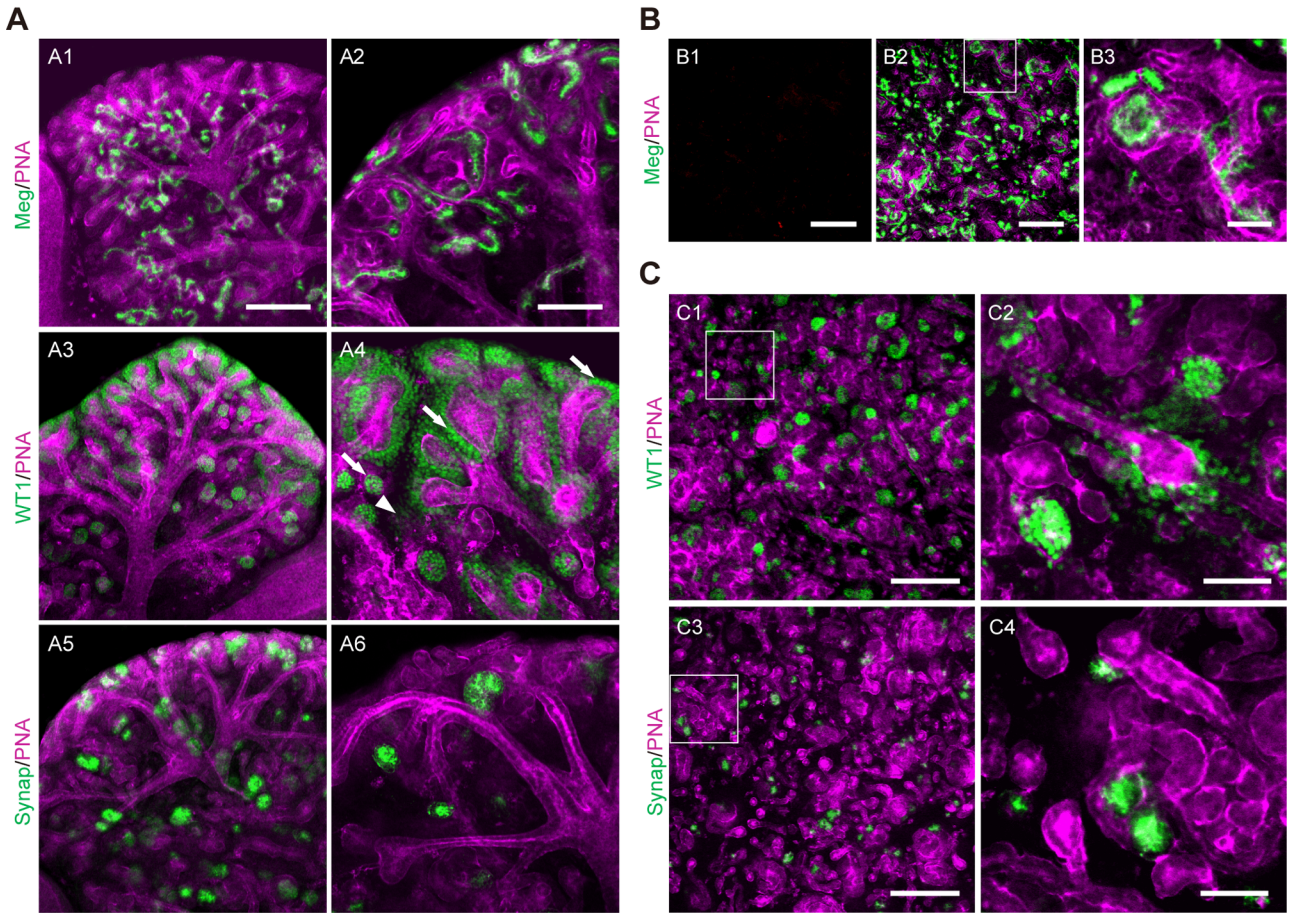

Fig. 4. Development of intact E13.5 mouse embryonic kidney and re-aggregated kidney rudiments cultured *ex vivo* for 5 days. (A) Representative confocal photomicrographs of intact kidney showed that proximal tubules were positively stained for megalin (Meg, green) and PNA (magenta). Developing glomeruli were positively stained for Wt1 (green) and synaptopodin (Synap, green). Arrows point to developing podocytes and the arrowhead points to MM. (B) E13.5 mouse embryonic kidneys were dissociated and pelleted as aggregates comprising 2×10^5 cells for each rudiment. Representative confocal photomicrographs of the re-aggregated rudiments cultured *ex vivo* at days 0 (B1) and 5 (B2–B3) showed that tubule-like structures formed during the 5-day culture. (C) The re-aggregated rudiments contain tubules and nascent glomerular-like structures that are similar to those of the intact rudiments cultured for 5 days. Boxed regions are shown enlarged in the magnified image to the right. Data were collected from three biological replicates. Scale bars: 200 µm (A1, A3,A5,B1,B2,C1,C3); 100 µm (A2,A4,A6); 50 µm (B3,C2,C4).

Biology Open (2018) 7, bio031799. doi:10.1242/bio.031799

dissociated kidney rudiment cells were pelleted and cultured *ex vivo* prior to staining with the aforementioned markers. Firstly, it was important to confirm that the disaggregation process was effective and that no non-dissociated renal structures were present at the start of the culture period. Therefore, at day 0, rudiments were stained for megalin and PNA. The results showed that no staining was present at day 0, whereas multiple tubular structures were present by day 5 (Fig. 4B). More detailed analysis of the re-aggregated rudiments showed that the pattern of tubular structures and nascent glomeruli appeared similar to that of the intact rudiments, which was consistent with previous studies (Kuzma-Kuzniarska et al., 2012; Rak-Raszewska et al., 2012; Ranghini et al., 2013). Although UB tubules formed, they did not form a contiguous UB tree (Fig. 4C).

The behaviour of mESC-derived *Bra*-GFP$^+$ cells within chimeric kidney rudiments cultured *ex vivo*

Before assessing the differentiation potential of the mESC-derived *Bra*$^+$ cells in the chimeric rudiment assay, it was first necessary to confirm that chimeric rudiments comprising a positive control cell population developed as expected. To this end, chimeric rudiments containing GFP$^+$ mouse neonatal kidney-derived stem cells (KSCs) were generated, as we have previously shown that KSCs can generate proximal tubule cells and podocytes within rudiments (E. Ranghini, Evaluating the expression profile and developmental potential of mouse kidney-derived stem cells, PhD thesis, University of Liverpool, 2011; Ranghini et al., 2013). The chimeric rudiments were cultured for 5 days *ex vivo* and analysed as previously using the renal cell-specific markers. On day 0, the KSCs were evenly distributed in the chimeric rudiments (Fig. S3). After 5 days of culture, the chimeric rudiments had developed proximal tubule-like structures that stained positively for megalin, as well as nascent glomeruli that contained podocytes, as evidenced by positive staining for Wt1 and synaptopodin. KSCs showed integration into the tubules and glomeruli of the developing nephrons (Figs 5–7).

To investigate the behaviour of mESC-derived *Bra*-GFP$^+$ cells within chimeric kidney rudiments cultured *ex vivo*. Firstly, the behaviour of E2-Crimson-expressing (E2C$^+$) *Bra*-GFP$^+$ cells isolated from mESC-derived EBs (3-D culture system) were investigated in the *ex vivo* rudiment assay. Staining for PNA, megalin, Wt1 and synaptopodin showed that similarly to the positive control chimeras comprising KSCs, the re-aggregated metanephric cells were able to develop tubular structures and nascent glomeruli (Figs 5–7). However, immunostaining for E2C showed that the EB-derived cells did not integrate into tubules or glomeruli, and instead, appeared to elongate and form interconnected cell networks throughout the rudiment. In many cases, the EB-derived cells appeared to align against the outer surface of developing glomeruli (Figs 5–7).

Next, the behaviour of E2C$^+$ *Bra*-GFP$^+$ cells isolated from the 2-D culture system was investigated using the chimeric rudiment assay. As with the EB-derived *Bra*-GFP$^+$ chimeras, staining for PNA, megalin, Wt1 and synaptopodin showed that re-aggregated metanephric cells in chimeras comprising *Bra*-GFP$^+$ cells isolated from the 2-D culture system were able to generate tubular structures and nascent glomeruli (Figs 5–7). Similarly to the E2C$^+$ EB-derived *Bra*-GFP$^+$ cells, the cells isolated from the 2-D culture system did not appear to integrate into tubules or glomeruli. However, in contrast to the EB-derived cells, those isolated from 2-D culture tended not to form connections with each other. Although elongated cells were occasionally observed in close proximity to developing glomeruli, the majority of the cells were not elongated and did not from interconnected cell networks (Figs 5–7). Furthermore, there appeared to be fewer E2C cells present in these chimeras compared to those generated from mESC-derived *Bra*-GFP$^+$ isolated from EBs.

The morphology of E2C$^+$ *Bra*-GFP$^+$ cells within the chimeras generated from EB-isolated cells appeared similar to that of endothelial cells within *ex vivo* kidney rudiments (Halt et al., 2016). To investigate if the E2C$^+$ cells had differentiated into endothelial cells, the rudiments were immunostained for the endothelial marker platelet and endothelial cell adhesion molecule 1 (PECAM-1) (Kondo et al., 2007). It was found that the metanephric cells generated PECAM-1$^+$ interconnected cell networks in both types of chimeric rudiment, indicating that endothelial cells had differentiated. Analysis of E2C$^+$ cells within the chimeric rudiments generated from EB-derived *Bra*-GFP$^+$ cells showed that the majority of these cells appeared to stain positively for PECAM-1, suggesting that they had differentiated into endothelial cells. In contrast, most of the E2C$^+$ cells within the chimeric rudiments generated from 2-D culture-derived *Bra*-GFP$^+$ cells did not stain positively for PECAM-1. Instead, only the elongated cells which were occasionally observed within these chimeras were found to stain for PECAM-1 (Fig. 8; Movies 2 and 3).

DISCUSSION

In this study, we generated mesoderm populations from a *Bra-GFP/Rosa26-E2C* mESC reporter line using 3-D and 2-D culture systems.

The dynamics of GFP expression during EB culture was similar to what has been previously observed in our group (A. Rak-Raszewska, Investigating the nephrogenic potential of mouse embryonic stem cells and their derivatives, PhD thesis, University of Liverpool, 2010); i.e. at low seeding density, GFP appeared to peak earlier than at higher seeding densities. A possible explanation is that mESCs might express inhibitors of mesoderm differentiation, such as noggin, which would be present at higher levels in higher density cultures, and might therefore delay mesoderm differentiation (GFP expression) (Tonegawa and Takahashi, 1998; Gratsch and O'Shea, 2002). Also, GFP expression was detected in EBs generated at low density that had not cavitated. This is similar to our laboratory's previous findings using the same *E14-Bra-GFP* mESC line, but with a different culture protocol developed by Fehling et al. (Fehling et al., 2003; Rak-Raszewska et al., 2012). In that study, GFP was only expressed within the EBs during days 3 to 4 with ∼60% of the population expressing GFP at day 4 (A. Rak-Raszewska, PhD thesis, 2010). This is much higher than the proportion we observed in the current study (less than 40%). However, EBs generated using Fehling's method did not form a proamniotic-like cavity, extra-embryonic endoderm or basement membranes. It is therefore envisaged that the properties of *Bra*$^+$ mesoderm cells generated from the two types of EBs (i.e. cavitating or non-cavitating), might have different properties and differentiation potential.

An interesting finding from the qRT-PCR analysis was that the expression levels of *Bra* in the GFP$^+$ cells isolated from the 3-D system were ∼50 times higher than in the GFP$^-$ cells, but *Bra* levels in GFP$^+$ cells isolated from the 2-D system were only approximately three times higher than in the corresponding GFP$^-$ cells. Yet, despite this, when *Bra* levels in the GFP$^+$ cells from the 3-D system were directly compared with levels in GFP$^+$ cells from the 2-D system, there was no significant difference. A possible explanation for this is that the GFP$^-$ cells in the EBs are likely to be endoderm or ectoderm cells that do not express *Bra*, whereas in the 2-D system, it is possible that the GFP$^-$ cells might be committed to the mesodermal lineage and have started to up-regulate *Bra*, but due to the time-lag between transcription and translation, might not have yet started to produce GFP. If this were the case, such cells would be

Biology Open (2018) 7, bio031799. doi:10.1242/bio.031799

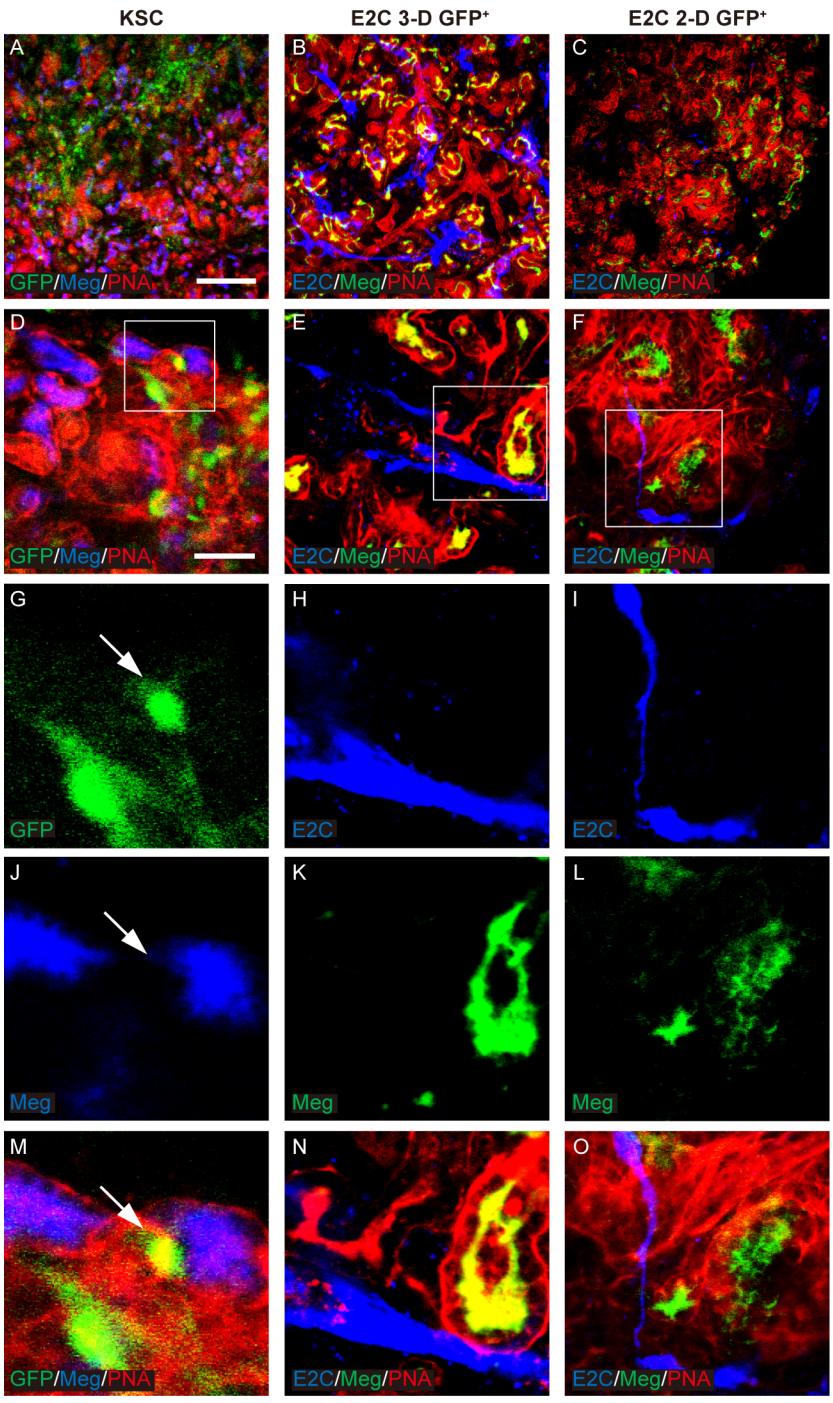

Fig. 5. Potential of *Bra-GFP*/*Rosa26-E2C* mESCs isolated from 3-D and 2-D systems to integrate in megalin-expressing renal tubules. (A-O) Rudiments were cultured *ex vivo* for 5 days. GFP-KSCs (green) were used as positive controls and showed integration into the tubules of the developing nephrons. Arrows point to the GFP$^+$ KSCs that had integrated into developing tubules that were dual stained by PNA (red) and megalin (Meg, blue) (G,J,M). In the day 5 chimeric rudiments comprising *Bra*-GFP$^+$ cells derived from mESC 3-D system, E2C$^+$ *Bra*-GFP$^+$ cells (blue) appeared to be elongated and formed an interconnected network within the rudiments. They were often found surrounding the tubules but did not integrate into them (B,E,H,K,N). In the day 5 chimeric rudiments comprising *Bra*-GFP$^+$ cells isolated from mESC 2-D system, fewer *Bra*-GFP$^+$ cells (blue) were observed, and, unlike those from the 3-D system, most did not appear to be elongated (C,F,I,L,O). Boxed regions are shown enlarged in the magnified images in the bottom row. Data were collected from three biological replicates. Scale bars: 200 µm (A–C) and 50 µm (D–F).

Bra$^+$ but GFP$^-$, and would thus have been sorted into the GFP-negative fraction by FACS.

When comparing the expression levels of key genes between the GFP$^+$ cells from the 3-D and 2-D systems, there were only three genes that were significantly up-regulated in the cells from the 3-D system, namely, *Foxf1*, *Cdx2* and *Hoxb1*. The high expression levels of *Foxf1* might suggest that the GFP$^+$ cells from the 3-D system might be lateral plate mesoderm cells. It is known that high levels of BMPs promote the differentiation of lateral plate mesoderm, whereas low levels of BMPs promote intermediate mesoderm (Tonegawa and Takahashi, 1998). It is therefore possible that in the larger cavitating EBs, there might be higher levels of BMPs which would then drive the differentiation of lateral plate mesoderm. However, the cells also had significantly higher levels of the nascent mesoderm gene, *Cdx2*, and the posterior mesoderm gene, *Hoxb1*. Additionally, *Cdx2*, *Foxf1* and *Hoxb1* are also expressed in the extra-embryonic mesoderm (Beck et al., 1995; Deschamps et al., 1999; Mahlapuu et al., 2001; Forlani et al., 2003; Chawengsaksophak et al., 2004), and therefore it might also be possible that these cells have adopted an extra-embryonic mesoderm fate. Furthermore, although not significant, there was a clear trend that the *Hox* genes tested, which are expressed in intermediate mesoderm, were up-regulated in the cells from the 3-D system. It is also possible that the timing of key gene expression in the *Brachyury*$^+$ cells under 3-D and 2-D culture conditions might result in varied differentiation rates.

Biology Open (2018) 7, bio031799. doi:10.1242/bio.031799

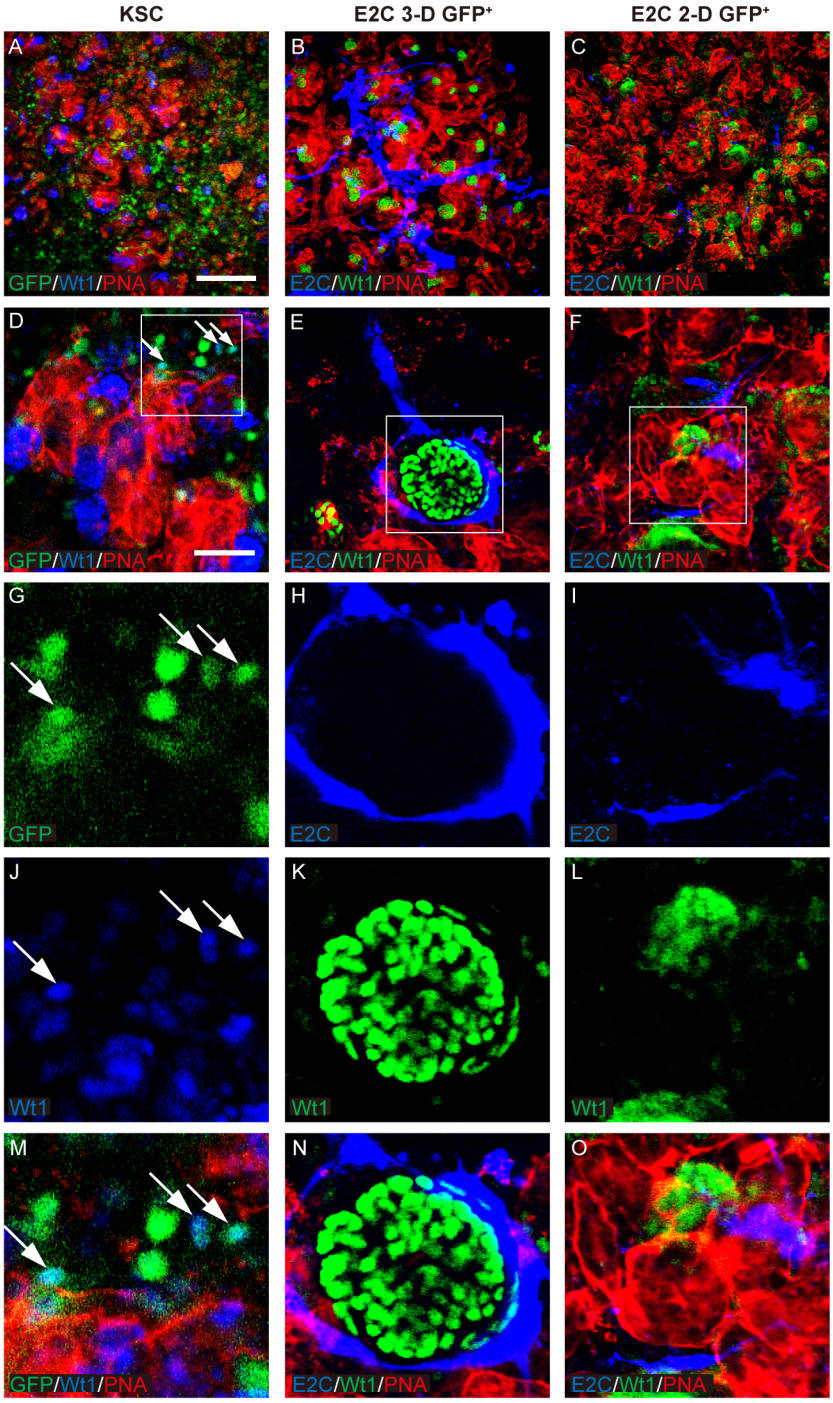

Fig. 6. Potential of *Bra-GFP*/*Rosa26-E2C* mESCs isolated from 3-D and 2-D systems to integrate into Wt1-expressing nascent glomeruli. (A-O) Rudiments were cultured *ex vivo* for 5 days. Arrows point to the integrated KSCs (positive controls) that were GFP-labelled and dual stained by PNA (red) and Wt1 (blue) (D,G,J,M). E2C$^+$ *Bra*-GFP$^+$ cells (blue) in the day 5 chimeric rudiments comprising *Bra*-GFP$^+$ cells derived from mESC 3-D system were often found surrounding the tubules (red) and glomerular structures (green) but did not integrate into them (B,E,H,K,N). *Bra*-GFP$^+$ cells isolated from mESC 2-D system also did not appear to integrate into any renal structures (C,F,I,L,O). Boxed regions are shown enlarged in the magnified images in the bottom row. Data were collected from three biological replicates. Scale bars: 200 µm (A–C); 50 µm (D–F).

By introducing the E2C-expressing mesodermal cells into the chimeric rudiments *ex vivo*, we showed that neither the *Bra*-GFP$^+$ cells derived from the 3-D nor 2-D culture systems appeared to integrate into the developing nephrons. The results are strikingly different from our laboratory's previous studies that investigated the nephrogenic potential of *Bra*-GFP$^+$ cells isolated from non-cavitating EBs in the same rudiment culture assay (Rak-Raszewska et al., 2012). In these earlier studies, it was found that *Bra*-GFP$^+$ mESCs derived from non-cavitating EBs were able to integrate into both the developing nephrons and UBs, and could form functional proximal tubule cells and podocytes (Rak-Raszewska et al., 2012). Another study by Vigneau et al. showed that *Bra*$^+$ cells derived from mouse EBs contributed to the proximal tubules when injected into the neonatal mouse kidney *in vivo* (Vigneau et al., 2007). The results we obtained with the *Bra*-GFP$^+$ cells obtained from cavitating EBs were surprising. We had expected that as these cells were isolated at a later time point than the *Bra*-GFP$^+$ cells in the non-cavitating EBs, they might more closely resemble posterior mesoderm, which has recently been shown to generate the MM but not the UB (Taguchi et al., 2014). We therefore thought that these cells might integrate into developing nephrons, but not the UBs. However, they did not integrate into either of these structures and instead appeared to differentiate into endothelial cells. There have been contrasting reports concerning the presence of endothelial cells in mouse kidney rudiments cultured *ex vivo*, with some studies suggesting that endothelial cells

Biology Open (2018) 7, bio031799. doi:10.1242/bio.031799

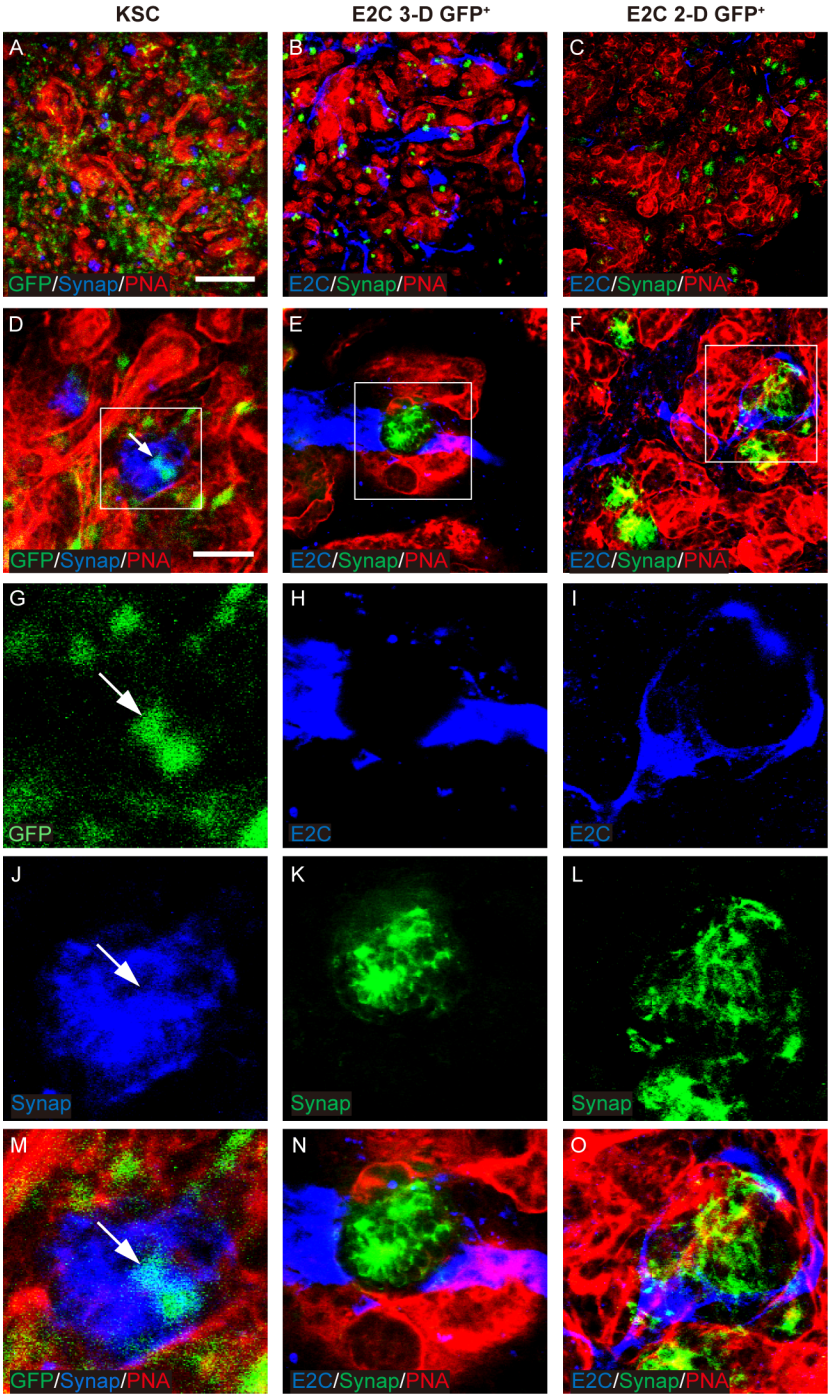

Fig. 7. Potential of *Bra-GFP*/*Rosa26-E2C* mESCs isolated from 3-D and 2-D systems to differentiate into synaptopodin-expressing podocytes. (A-O) Rudiments were cultured *ex vivo* for 5 days. Arrows point to the integrated KSCs (positive controls) that were GFP-labelled and dual stained with PNA (red) and synaptopodin (Synap, blue) (D,G,J,M). In the day 5 chimeric rudiments comprising *Bra*-GFP$^+$ cells derived from mESC 3-D system, E2C$^+$ *Bra*-GFP$^+$ cells (blue) did not generate synaptopodin$^+$ cells (B,E,H,K,N). *Bra*-GFP$^+$ cells isolated from mESC 2-D system (blue) also failed to generate synaptopodin$^+$ cells (C,F,I,L,O). Boxed regions are shown enlarged in the magnified images in the bottom row. Data were collected from three biological replicates. Scale bars: 200 µm (A–C) and 50 µm (D–F).

cannot survive in *ex vivo* rudiments (Loughna et al., 1997) and others suggesting that they do (Halt et al., 2016). Our findings are consistent with the Halt et al. study that indicates that endothelial cells are present in rudiments and, similarly to that study, we found that although the endothelial cells formed interconnected networks, they did not form capillaries with lumen, nor did they invest the developing glomeruli.

The key differences in the gene expression profile of the *Bra*-GFP$^+$ cells isolated from cavitating EBs (current study) and non-cavitating EBs (previous study) (A. Rak-Raszewska, PhD thesis, 2010) is that in comparison to GFP$^-$ cells, the former expressed much higher levels of *Foxf1*, which is highly expressed in lateral plate mesoderm, and lower levels of the MM genes, *Gdnf* and *Osr1* (A. Rak-Raszewska, PhD thesis, 2010). The high expression levels of *Foxf1* might explain why the EB-derived *Bra*-GFP$^+$ cells in the current study had a tendency to generate endothelial cells, because it is known that *Foxf1* is essential for vasculogenesis in the developing embryo and is expressed in endothelial cells (Mahlapuu et al., 2001; Ren et al., 2014).

High levels of BMP signals and their receptors ALK3/6 have been shown to promote a lateral plate mesoderm fate (James and Schultheiss, 2005). Due to the heterogeneous nature of the EBs, it is possible that mesoderm niches that resemble dynamic microenvironments of the *in vivo* primitive streak have been formed. Cells residing in the niches that are exposed to high concentrations of BMP signals might, therefore, adopt a lateral plate

Biology Open (2018) 7, bio031799. doi:10.1242/bio.031799

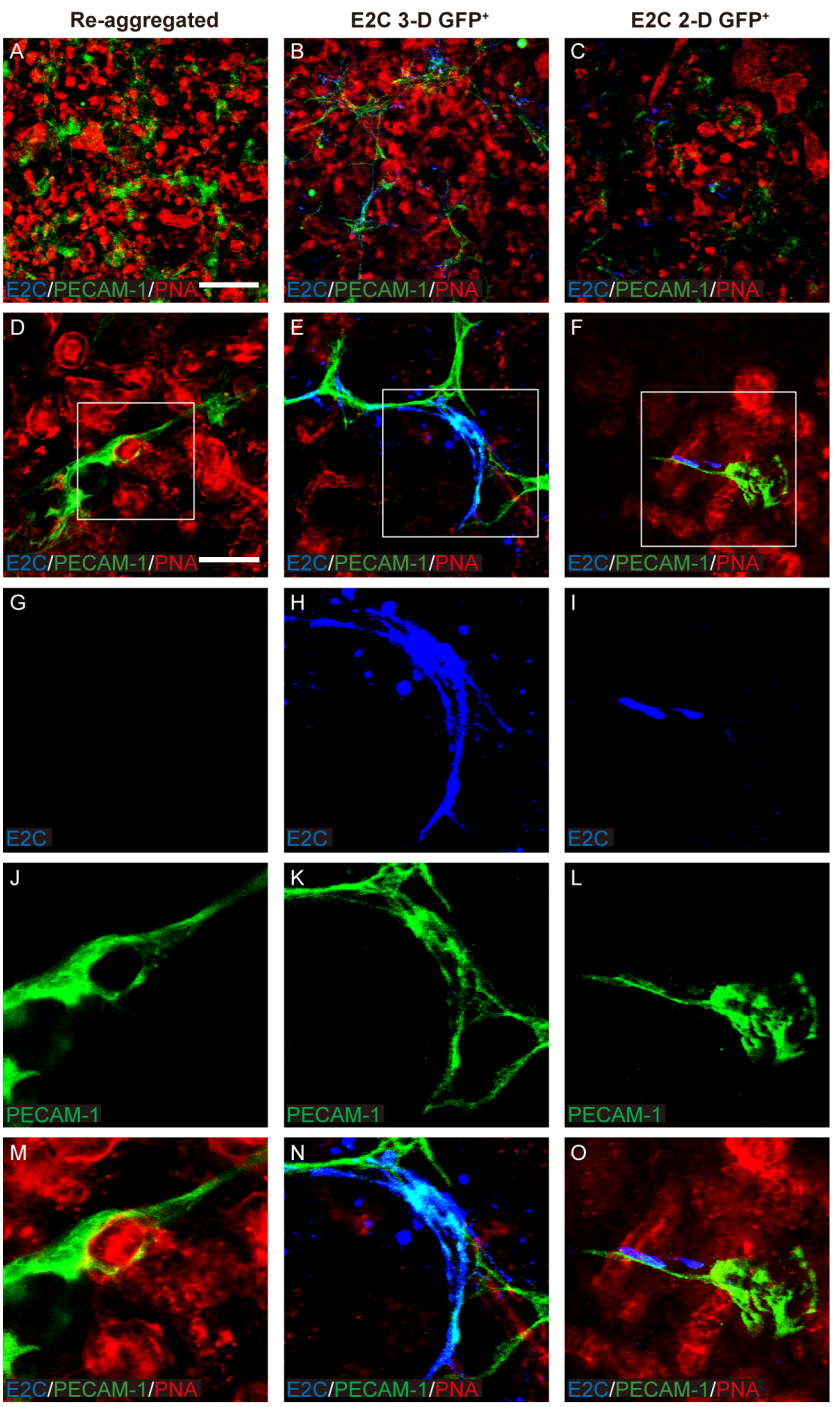

Fig. 8. Confocal photomicrographs showing PECAM-1 immunostaining within day 5 *ex vivo* mouse embryonic kidney rudiments comprising *Bra*-GFP$^+$ derived from *Bra-GFP*/*Rosa26-E2C* mESCs cultured in 3-D and 2-D systems. (A-O) Immunostaining for E2C was undertaken to identify the mesodermal cells, and PECAM-1 immunostaining was performed to identify endothelial-like cells. (A,D,G,J,M) Re-aggregated rudiments without exogenous cells; (B,E,H,K,N) re-aggregated chimeric rudiments containing E2C$^+$ *Bra*-GFP$^+$ cells isolated from the 3-D culture system; (C,F,I,L,O) re-aggregated chimeric rudiments containing E2C$^+$ *Bra*-GFP$^+$ cells isolated from the 2-D culture system. Boxed regions are shown enlarged in the magnified images in the bottom row. Data were collected from three biological replicates. Scale bars: 200 µm (A–C); 50 µm (D–F).

mesoderm fate. Retinoic acid, FGF and Wnt signals might also affect the cell commitment of lateral plate mesoderm but their effects may be stochastic within the EBs. Nevertheless, we cannot exclude the possibility that the timing might have been another factor; for instance, *Bra*-GFP$^+$ cells isolated at slightly earlier or later time-points might have expressed genes of other mesodermal lineages.

Regarding the *Bra*-GFP$^+$ isolated from the 2-D system, it was found that these also did not integrate into developing nephrons or UBs. Furthermore, only a small proportion of these cells appeared to differentiate into endothelial cells. The majority of the cells did not form interconnected cell networks and appeared to be randomly dispersed throughout the stroma. Similarly to the *Bra*-GFP$^+$ cells from the cavitating EBs, the *Bra*-GFP$^+$ cells from the 2-D system did not show any noticeable up-regulation of *Gdnf* or *Osr1* in comparison with the *Bra*-GFP$^-$ cells. However, in contrast to the EB-derived cells, those isolated from the 2-D system did not show up-regulation of *Foxf1*, which is consistent with their limited tendency to generate endothelial cells. It is possible that the *Bra*-GFP$^+$ cells from the 2-D system might have differentiated into stromal cells, but it was not possible to test this due to the lack of a stroma-specific antibody. It is interesting to note that the *Bra*-GFP$^+$ cells from the 2-D system expressed higher levels of the stromal gene, *Foxd1* (Mugford et al., 2008) compared to those from the 3-D system, but the results were not statistically significant.

Biology Open (2018) 7, bio031799. doi:10.1242/bio.031799

MATERIALS AND METHODS

Routine cell culture

Bra-GFP/Rosa26-E2C mESCs (Zhou et al., 2018) were maintained in 0.1% gelatinised six-well tissue culture plates with mitomycin-C (Sigma-Aldrich, M4287) inactivated STO (ATCC, SCRC-1049) feeder cells at 37°C in a humidified incubator with 5% CO_2 in Dulbecco's modified Eagle's medium (DMEM) (Sigma-Aldrich, D6546) supplemented with 15% fetal bovine serum (FBS) (Sigma-Aldrich, F2442), 1% minimum essential medium (MEM) non-essential amino acid (Sigma-Aldrich, M7145), 2 mmol l^{-1} L-glutamine (Sigma-Aldrich, G7513), 0.1 mmol l^{-1} β-mercaptoethanol (Gibco, 31350) and 1000 U ml^{-1} mouse leukaemia inhibitory factor (mLIF) (Merck Millipore, ESG1107). Cells were passaged every other day and those at passage 13–22 were used for experiments.

GFP-expressing mouse neonatal kidney-derived stem cells (GFP-KSCs) (E. Ranghini, PhD thesis, 2011) were maintained in 60-mm tissue culture dishes at 37°C in a humidified incubator with 5% CO_2 in DMEM supplemented with 10% FBS (Gibco, 10270), 1% MEM non-essential amino acid (Sigma-Aldrich, M7145), 2 mmol l^{-1} L-glutamine (Sigma-Aldrich, G7513) and 0.1 mmol l^{-1} β-mercaptoethanol (Gibco, 31350). Cells were passaged 2–3 times per week and those at passage 17–20 were used for experiments.

3-D EB system

mESCs were sub-cultured in gelatinised six-well tissue culture plates for 48 h to deplete feeder cells. Cells were then collected and seeded in 90-mm bacterial petri dishes (Sterilin, Newport, UK; 101VR20) at the densities of 6.25×10^4, 1.25×10^5 and 2.5×10^5 cells ml^{-1} to form aggregates. The EBs were maintained at 37°C in a humidified incubator with 5% CO_2 in DMEM supplemented with 10% FBS (Sigma-Aldrich, F2442), 1% MEM non-essential amino acid, 2 mmol l^{-1} L-glutamine and 0.1 mmol l^{-1} β-mercaptoethanol for up to 9 days with a medium change every other day. Each dish was split 1:2 on day 3 and EB morphology was examined on days 4 and 7. Experiments were performed in three independent biological replicates.

2-D system

mESCs were sub-cultured in gelatinised six-well tissue culture plates for 48 h to deplete feeder cells. Cells were collected and plated into gelatinised six-well plates at 1×10^5 cells per cm^2 for 24 h. 2-D induction culture was based on the protocols previously described (Turner et al., 2014a,b). Briefly, cells were then harvested and re-plated into 60-mm tissue culture dishes at a density of 4.7×10^3 cells per cm^2 with overnight incubation in mESC culture medium. The following morning, medium was changed to NDiff® 227 (Clontech, Saint-Germain-en-Laye, France; Y40002) for 48 h and then to NDiff® 227 supplemented with Activin-A (R&D Systems, Abingdon, UK; 338-AC) and CHIR 99021 (Tocris, Abingdon, UK; 4423) to a final concentration of 100 ng ml^{-1} and 3 µmol l^{-1}, respectively, for a further 48 h incubation. Medium was changed on a daily basis. Experiments were carried out in three independent biological replicates.

Cell-IQ real-time imaging

On day 3, EBs that were formed from mESCs at a plating density of 1.25×10^5 cells ml^{-1} were harvested and plated onto solidified 2% agarose gel (Sigma-Aldrich, A9045) in glass bottom six-well plates (MatTek, Bratislava, Slovakia; P06G-0-20-F). They were then embedded in a thin overlay of 1% agarose. Each well was filled with 3 ml EB medium once the overlaid gels were set. Plates were maintained in a Cell-IQ (Chip-Man Technologies Ltd) imaging facility. EBs were imaged by the Cell-IQ Imagen (Chip-Man Technologies Ltd) software on days 3 to 9 on an hourly basis. Imaging data from both bright field and 488 nm laser for the GFP fluorescence signal were documented from three independent biological replicates. Raw data were analysed by the Cell-IQ Analyser (Chip-Man Technologies Ltd) and ImageJ (https://imagej.nih.gov/ij/) software.

EB fixation and cryo-sectioning

EBs were harvested on day 7 and fixed with 4% paraformaldehyde (PFA). They were then soaked in 15% sucrose followed by embedding in the 7.5% molten gelatin. Samples were mounted onto cork disks with Shandon™ Cryomatrix™ embedding resin (Thermo Fisher Scientific, 6769006) and cut with a cryostat at 20 µm.

Flow cytometry analysis

Single-cell suspensions of 1×10^6 cells ml^{-1} were obtained from 3-D or 2-D culture systems and examined by a BD FACScalibur (BD Biosciences) flow cytometer according to the manufacturer's instructions, using a 488-nm laser to detect the GFP signal. For analysis of the GFP expression window in the EBs, wild-type E14TG2a-derived EBs were used as a negative control. For analysis of GFP expression in the 2-D system, undifferentiated *Bra-GFP/Rosa26-E2C* mESCs sub-cultured in gelatinised dishes in mESC medium for 24 h prior to induction were used as a negative control. Data were acquired from two biological replicates by the BD CellQuest (BD Biosciences) software based on 10^4 events and analysed using Cyflogic (http://www.cyflogic.com/) software.

FACS

Single-cell suspensions of 1×10^7 cells ml^{-1} were obtained from day 6 3-D EBs or day 4 2-D monolayer cultures. Sorting was performed to isolate *Bra*-GFP$^+$ cells using the BD FACSAria (BD Biosciences) flow sorter with the 530/30 bandpass filter and 502 longpass mirror. Day 6 EBs derived from wild-type E14TG2a mESCs and undifferentiated *Bra-GFP/Rosa26-E2C* mESCs sub-cultured in gelatinised dishes for 24 h prior to induced differentiation were used as negative controls for 3-D and 2-D systems, respectively. Data output was performed using BD FACSDiva (version 6.1.3) software. Experiments were performed in three independent biological replicates.

qRT-PCR and statistical analysis

Cell lysis of FACS-sorted *Bra*-GFP$^+$ populations, reverse transcription and quantitative polymerase chain reaction (qPCR) amplification was performed using the Fast SYBR® Green Cells-to-CT™ Kit (Thermo Fisher Scientific, 4405659) in accordance with the manufacturer's instructions. Gene transcription was detected by a CFX Connect Real-time PCR Detection System (Bio-Rad) using specific primers validated in house (Table S2). The reaction was set up with the following steps: 95°C for 20 s initial DNA polymerase activation followed by 40 cycles of denaturation at 95°C for 3 s and annealing/extension at 60°C for 30 s. qPCR specificity was assessed by melt curves and then verified by agarose gel electrophoresis. Non-template control was performed for each analysed gene and the non-reverse transcriptase control was also included to verify the elimination of genomic DNA. Three biological replicates for the *Bra*-GFP$^+$ populations isolated from 3-D and 2-D systems, and two biological replicates for *Bra*-GFP$^-$ populations derived from the 3-D and 2-D systems were assessed. For each reaction product analysed, two technical replicates were prepared. Data were acquired using the incorporated Bio-Rad CFX Manager (version 3.1) software. Relative gene expression levels normalised to two endogenous reference genes *Gapdh* and *β-actin* ($\Delta\Delta C_t$) and statistical analysis were also performed using two-tailed Student's *t*-test by the same software, where $P<0.05$ was considered statistically significant.

Mouse embryonic kidney rudiment *ex vivo* culture

The mouse embryonic kidney rudiment *ex vivo* culture was based on the protocols previously described (Unbekandt and Davies, 2010). Briefly, kidneys were dissected out from embryonic day (E) 13.5 CD1 mouse (Charles River) and dissociated into single cells following an incubation of 15 min in 0.25% trypsin/PBS (Sigma-Aldrich, T4174) with intermittent gentle agitation. Cells were pelleted at 1 800× ***g*** for 2 min and re-suspended in kidney rudiment medium comprising MEME (Sigma-Aldrich, M5650) and 10% FBS. In the meantime, FACS-sorted *Bra*-GFP$^+$ cells derived from mESC 3-D or 2-D systems were collected in rudiment medium and counted. A total of 2×10^5 cells were used in each rudiment, wherein kidney rudiment cells and *Bra*-GFP$^+$ cells were mixed at a ratio of 1:9. Rudiments were cultured with Rho-associated, coiled-coil containing protein kinase inhibitor (ROCKi, Y-27632, Merck Millipore, 688001) for 24 h followed by a further 4 days in the absence of ROCKi. Controls were also set up, including kidney rudiments comprising GFP-KSCs (1:9 ratio of KSC: kidney rudiment cells),

reaggregated kidney rudiments (formed by kidney rudiment cells only), and intact kidney rudiments. Experiments were performed in three independent biological replicates.

Immunofluorescence staining

For EB frozen section assay, sections were blocked in 10% serum solution and incubated with E2C primary and secondary antibodies, followed by nuclear counter-staining of 4′,6-diamidino-2-phenylindole (DAPI, Thermo Fisher Scientific, D1306, 1/100,000). Slides were mounted with DAKO fluorescent mounting medium (Agilent Technologies, Cheadle, UK; S3023) and sealed for viewing on the DM2500 (Leica, Milton Keynes, UK) fluorescence microscope with a 40× objective and appropriate excitation and emission filter sets. Data were acquired using the Leica Application Suite (LAS, Leica) integrated software and analysed by ImageJ software.

For mouse embryonic kidney rudiments assay, immunofluorescence and image analysis were carried out based on the protocols described previously (Rak-Raszewska et al., 2012; Ranghini et al., 2013). Briefly, rudiments of days 0 and 5 were fixed with 4% PFA and blocked with 10% serum solution containing 0.1% Triton X-100, followed by incubation with primary antibodies for E2C, megalin, Wt1, synaptopodin and PECAM-1, where necessary. They were then incubated with secondary antibodies followed by counter-staining of 10 µg μl^{-1} PNA (Vector Laboratories, Peterborough, UK; RL-1072). Controls were also included as above to check for non-specific binding of secondary antibodies. Samples were mounted with DAKO fluorescent mounting medium (Agilent Technologies, S3023) and sealed. Data were acquired using a LSM 510 META (Zeiss, Cambridge, UK) multiphoton confocal laser scanning microscope with a 40× oil immersion, 20× or 10× lens and appropriate excitation and emission filter sets. Image data analysis was performed by ImageJ and Imaris (Bitplane, version 9.0.2) software.

The following primary antibodies were used: rabbit polyclonal IgG E2C (Clontech; 632496, 1/1 000), mouse monoclonal megalin IgG1 (Acris, Upper Heyford, UK; DM3613P, 1/200), mouse monoclonal Wt1 (Millipore, 05–753, 1/100), mouse monoclonal synaptopodin IgG_1 (Progen, Heidelberg, Germany; 65194, 1/2), rat monoclonal PECAM (BD Pharmingen, San Diego, USA; 550274, 1/100). Secondary antibodies used were Alexa Fluor (AF) 488-conjugated chicken anti-rabbit IgG (Thermo Fisher Scientific, AF A21441, 1/1000), AF594 goat anti-rabbit (Thermo Fisher Scientific, AF A11012, 1/1000), AF488 goat anti-mouse IgG_1 (Thermo Fisher Scientific, AF A21121, 1/1000), AF647 donkey anti-mouse IgG (H+L) (Thermo Fisher Scientific, AF A31571, 1/1000), and AF488 donkey anti-rat IgG (H+L) (Thermo Fisher Scientific, AF A21208, 1/1000).

Acknowledgements

We thank Dr Sandra Pereira Cachinho for help with FACS, Dr Marco Marcello and Dr Joanna Wnetrzak for assistance with confocal laser scanning microscopy, Dr Sumaya Dauleh for help with the rudiment assay, and Dr David Mason for advice on 3-D microscopy image processing. We also acknowledge support from the Biomedical Services Unit, the Cell Sorting and Isolation Facilities and the Centre for Cell Imaging of the Technology Directorate at the University of Liverpool.

Competing interests

The authors declare no competing or financial interests.

Author contributions

Conceptualization: P.M.; Methodology: J.Z., P.M.; Validation: J.Z.; Formal analysis: J.Z.; Investigation: J.Z.; Resources: A.P.; Writing - original draft: J.Z.; Writing - review & editing: A.P., P.M.; Visualization: J.Z.; Supervision: P.M.; Funding acquisition: J.Z., P.M.

Funding

This work was supported by the China Scholarship Council [20123024 to J.Z.]; and the UK Regenerative Medicine Platform (UKRMP) hub, 'Safety and Efficacy, focussing on Imaging Technologies' (jointly funded by the Medical Research Council, the Engineering and Physical Sciences Research Council and the Biotechnology and Biological Sciences Research Council) [MR/K026739/1].

Supplementary information

Supplementary information available online at
http://bio.biologists.org/lookup/doi/10.1242/bio.031799.supplemental

References

Arnold, S. J. and Robertson, E. J. (2009). Making a commitment: cell lineage allocation and axis patterning in the early mouse embryo. *Nat. Rev. Mol. Cell Biol.* **10**, 91-103.

Basson, M. A., Watson-Johnson, J., Shakya, R., Akbulut, S., Hyink, D., Costantini, F. D., Wilson, P. D., Mason, I. J. and Licht, J. D. (2006). Branching morphogenesis of the ureteric epithelium during kidney development is coordinated by the opposing functions of GDNF and Sprouty1. *Dev. Biol.* **299**, 466-477.

Beck, F., Erler, T., Russell, A. and James, R. (1995). Expression of *Cdx-2* in the mouse embryo and placenta: possible role in patterning of the extra-embryonic membranes. *Dev. Dyn.* **204**, 219-227.

Blancas, A. A., Shih, A. J., Lauer, N. E. and McCloskey, K. E. (2011). Endothelial cells from embryonic stem cells in a chemically defined medium. *Stem Cells Dev.* **20**, 2153-2161.

Blancas, A. A., Wong, L. E., Glaser, D. E. and McCloskey, K. E. (2013). Specialized tip/stalk-like and phalanx-like endothelial cells from embryonic stem cells. *Stem Cells Dev.* **22**, 1398-1407.

Carapuço, M., Nóvoa, A., Bobola, N. and Mallo, M. (2005). *Hox* genes specify vertebral types in the presomitic mesoderm. *Genes Dev.* **19**, 2116-2121.

Chapman, D. L., Cooper-Morgan, A., Harrelson, Z. and Papaioannou, V. E. (2003). Critical role for *Tbx6* in mesoderm specification in the mouse embryo. *Mech. Dev.* **120**, 837-847.

Chawengsaksophak, K., de Graaff, W., Rossant, J., Deschamps, J. and Beck, F. (2004). *Cdx2* is essential for axial elongation in mouse development. *Proc. Natl. Acad. Sci. USA* **101**, 7641-7645.

Concepcion, D. and Papaioannou, V. E. (2014). Nature and extent of left/right axis defects in T^{Wis}/T^{Wis} mutant mouse embryos. *Dev. Dyn.* **243**, 1046-1053.

Conlon, F. L., Wright, C. V. E. and Robertson, E. J. (1995). Effects of the T^{Wis} mutation on notochord formation and mesodermal patterning. *Mech. Dev.* **49**, 201-209.

Dauleh, S., Santeramo, I., Fielding, C., Ward, K., Herrmann, A., Murray, P. and Wilm, B. (2016). Characterisation of cultured mesothelial cells derived from the murine adult omentum. *PLoS ONE* **11**, e0158997.

Deschamps, J., van den Akker, E., Forlani, S., De Graaff, W., Oosterveen, T., Roelen, B. and Roelfsema, J. (1999). Initiation, establishment and maintenance of *Hox* gene expression patterns in the mouse. *Int. J. Dev. Biol.* **43**, 635-650.

Doetschman, T. C., Eistetter, H., Katz, M., Schmidt, W. and Kemler, R. (1985). The *in vitro* development of blastocyst-derived embryonic stem cell lines: formation of visceral yolk sac, blood islands and myocardium. *J. Embryol. Exp. Morphol.* **87**, 27-45.

Dressler, G. R. (2009). Advances in early kidney specification, development and patterning. *Development* **136**, 3863-3874.

Erselius, J. R., Goulding, M. D. and Gruss, P. (1990). Structure and expression pattern of the murine *Hox-3.2* gene. *Development* **110**, 629-642.

Evans, M. J. and Kaufman, M. H. (1981). Establishment in culture of pluripotential cells from mouse embryos. *Nature* **292**, 154-156.

Fehling, H. J., Lacaud, G., Kubo, A., Kennedy, M., Robertson, S., Keller, G. and Kouskoff, V. (2003). Tracking mesoderm induction and its specification to the hemangioblast during embryonic stem cell differentiation. *Development* **130**, 4217-4227.

Forlani, S., Lawson, K. A. and Deschamps, J. (2003). Acquisition of Hox codes during gastrulation and axial elongation in the mouse embryo. *Development* **130**, 3807-3819.

Gadue, P., Huber, T. L., Paddison, P. J. and Keller, G. M. (2006). Wnt and TGF-β signaling are required for the induction of an *in vitro* model of primitive streak formation using embryonic stem cells. *Proc. Natl. Acad. Sci. USA* **103**, 16806-16811.

Gilbert, S. F. (2010). *Developmental Biology*. Sunderland: Sinauer Associates, Inc.

Gratsch, T. E. and O'Shea, K. S. (2002). Noggin and chordin have distinct activities in promoting lineage commitment of mouse embryonic stem (ES) cells. *Dev. Biol.* **245**, 83-94.

Halt, K. J., Pärssinen, H. E., Junttila, S. M., Saarela, U., Sims-Lucas, S., Koivunen, P., Myllyharju, J., Quaggin, S., Skovorodkin, I. N. and Vainio, S. J. (2016). $CD146^+$ cells are essential for kidney vasculature development. *Kidney Int.* **90**, 311-324.

Herrmann, B. G., Labeit, S., Poustka, A., King, T. R. and Lehrach, H. (1990). Cloning of the *T* gene required in mesoderm formation in the mouse. *Nature* **343**, 617-622.

James, R. G. and Schultheiss, T. M. (2005). Bmp signaling promotes intermediate mesoderm gene expression in a dose-dependent, cell-autonomous and translation-dependent manner. *Dev. Biol.* **288**, 113-125.

Keller, G., Kennedy, M., Papayannopoulou, T. and Wiles, M. V. (1993). Hematopoietic commitment during embryonic stem cell differentiation in culture. *Mol. Cell Biol.* **13**, 473-486.

King, T., Beddington, R. S. P. and Brown, N. A. (1998). The role of the *brachyury* gene in heart development and left–right specification in the mouse. *Mech. Dev.* **79**, 29-37.

Kispert, A. and Herrmann, B. G. (1994). Immunohistochemical Analysis of the Brachyury protein in wild-type and mutant mouse embryos. *Dev. Biol.* **161**, 179-193.
Kispert, A., Koschorz, B. and Herrmann, B. G. (1995). The T protein encoded by *Brachyury* is a tissue-specific transcription factor. *EMBO J.* **14**, 4763-4772.
Kmita, M., van Der Hoeven, F., Zákány, J., Krumlauf, R. and Duboule, D. (2000). Mechanisms of *Hox* gene colinearity: transposition of the anterior *Hoxb1* gene into the posterior *HoxD* complex. *Genes Dev.* **14**, 198-211.
Kondo, S., Scheef, E. A., Sheibani, N. and Sorenson, C. M. (2007). PECAM-1 isoform-specific regulation of kidney endothelial cell migration and capillary morphogenesis. *Am. J. Physiol. Cell Physiol.* **292**, C2070-C2083.
Kuzma-Kuzniarska, M., Rak-Raszewska, A., Kenny, S., Edgar, D., Wilm, B., Fuente Mora, C., Davies, J. A. and Murray, P. (2012). Integration potential of mouse and human bone marrow-derived mesenchymal stem cells. *Differentiation* **83**, 128-137.
Laitinen, L., Virtanen, I. and Saxén, L. (1987). Changes in the glycosylation pattern during embryonic development of mouse kidney as revealed with lectin conjugates. *J. Histochem. Cytochem.* **35**, 55-65.
Lin, L. F., Doherty, D. H., Lile, J. D., Bektesh, S. and Collins, F. (1993). GDNF: a glial cell line-derived neurotrophic factor for midbrain dopaminergic neurons. *Science* **260**, 1130-1132.
Little, M. H. (2015). *Kidney Development, Disease, Repair and Regeneration*. San Diego: Elsevier Science Publishing Co Inc.
Little, M. H., Combes, A. N. and Takasato, M. (2016). Understanding kidney morphogenesis to guide renal tissue regeneration. *Nat. Rev. Nephrol.* **12**, 624-635.
Loughna, S., Hardman, P., Landels, E., Jussila, L., Alitalo, K. and Woolf, A. S. (1997). A molecular and genetic analysis of renalglomerular capillary development. *Angiogenesis* **1**, 84-101.
Mahlapuu, M., Ormestad, M., Enerbäck, S. and Carlsson, P. (2001). The forkhead transcription factor *Foxf1* is required for differentiation of extra-embryonic and lateral plate mesoderm. *Development* **128**, 155-166.
Martin, G. R. (1981). Isolation of a pluripotent cell line from early mouse embryos cultured in medium conditioned by teratocarcinoma stem cells. *Proc. Natl. Acad. Sci. USA* **78**, 7634-7638.
Moore, A. W., McInnes, L., Kreidberg, J., Hastie, N. D. and Schedl, A. (1999). YAC complementation shows a requirement for *Wt1* in the development of epicardium, adrenal gland and throughout nephrogenesis. *Development* **126**, 1845-1857.
Mugford, J. W., Sipilä, P., McMahon, J. A. and McMahon, A. P. (2008). *Osr1* expression demarcates a multi-potent population of intermediate mesoderm that undergoes progressive restriction to an *Osr1*-dependent nephron progenitor compartment within the mammalian kidney. *Dev. Biol.* **324**, 88-98.
Mundel, P., Heid, H. W., Mundel, T. M., Krüger, M., Reiser, J. and Kriz, W. (1997). Synaptopodin: an actin-associated protein in telencephalic dendrites and renal podocytes. *J. Cell Biol.* **139**, 193-204.
Murray, P. and Edgar, D. (2000). Regulation of programmed cell death by basement membranes in embryonic development. *J. Cell Biol.* **150**, 1215-1221.
Murray, P. and Edgar, D. (2004). The topographical regulation of embryonic stem cell differentiation. *Philos. Trans. R. Soc. Lond. B Biol. Sci.* **359**, 1009-1020.
Papaioannou, V. E. (2014). The T-box gene family: emerging roles in development, stem cells and cancer. *Development* **141**, 3819-3833.
Pietilä, I. and Vainio, S. J. (2014). Kidney development: an overview. *Nephron Exp. Nephrol.* **126**, 40-44.
Rak-Raszewska, A., Wilm, B., Edgar, D., Kenny, S., Woolf, A. S. and Murray, P. (2012). Development of embryonic stem cells in recombinant kidneys. *Organogenesis* **8**, 125-136.
Ranghini, E., Mora, C. F., Edgar, D., Kenny, S. E., Murray, P. and Wilm, B. (2013). Stem cells derived from neonatal mouse kidney generate functional proximal tubule-like cells and integrate into developing nephrons *in vitro*. *PLoS ONE* **8**, e62953.
Ren, X., Ustiyan, V., Pradhan, A., Cai, Y., Havrilak, J. A., Bolte, C. S., Shannon, J. M., Kalin, T. V. and Kalinichenko, V. V. (2014). FOXF1 transcription factor is required for formation of embryonic vasculature by regulating VEGF signaling in endothelial cells. *Circ. Res.* **115**, 709-720.
Robertson, E. J. (1987). *Teratocarcinomas and Embryonic Stem Cells: A Practical Approach*. Oxford: IRL Press.
Rodriguez, T. A., Srinivas, S., Clements, M. P., Smith, J. C. and Beddington, R. S. (2005). Induction and migration of the anterior visceral endoderm is regulated by the extra-embryonic ectoderm. *Development* **132**, 2513-2520.
Sakurai, H., Inami, Y., Tamamura, Y., Yoshikai, T., Sehara-Fujisawa, A. and Isobe, K.-I. (2009). Bidirectional induction toward paraxial mesodermal derivatives from mouse ES cells in chemically defined medium. *Stem Cell Res.* **3**, 157-169.
Sánchez, M. P., Silos-Santiago, I., Frisén, J., He, B., Lira, S. A. and Barbacid, M. (1996). Renal agenesis and the absence of enteric neurons in mice lacking GDNF. *Nature* **382**, 70-73.
Savory, J. G. A., Bouchard, N., Pierre, V., Rijli, F. M., De Repentigny, Y., Kothary, R. and Lohnes, D. (2009). *Cdx2* regulation of posterior development through non-Hox targets. *Development* **136**, 4099-4110.
Shankland, S. J., Pippin, J. W., Reiser, J. and Mundel, P. (2007). Podocytes in culture: past, present, and future. *Kidney Int.* **72**, 26-36.
Shen, M. M. and Leder, P. (1992). Leukemia inhibitory factor is expressed by the preimplantation uterus and selectively blocks primitive ectoderm formation *in vitro*. *Proc. Natl. Acad. Sci. USA* **89**, 8240-8244.
Showell, C., Binder, O. and Conlon, F. L. (2004). T-box genes in early embryogenesis. *Dev. Dyn.* **229**, 201-218.
Stern, C. (2004). *Gastrulation: From Cells to Embryo*. New York: Cold Spring Harbor Laboratory Press.
Taguchi, A., Kaku, Y., Ohmori, T., Sharmin, S., Ogawa, M., Sasaki, H. and Nishinakamura, R. (2014). Redefining the *in vivo* origin of metanephric nephron progenitors enables generation of complex kidney structures from pluripotent stem cells. *Cell Stem Cell* **14**, 53-67.
Takasato, M., Er, P. X., Becroft, M., Vanslambrouck, J. M., Stanley, E. G., Elefanty, A. G. and Little, M. H. (2014). Directing human embryonic stem cell differentiation towards a renal lineage generates a self-organizing kidney. *Nat. Cell Biol.* **16**, 118-126.
Tonegawa, A. and Takahashi, Y. (1998). Somitogenesis controlled by Noggin. *Dev. Biol.* **202**, 172-182.
Turner, D. A., Rué, P., Mackenzie, J. P., Davies, E. and Martinez Arias, A. (2014a). Brachyury cooperates with Wnt/β-catenin signalling to elicit primitive-streak-like behaviour in differentiating mouse embryonic stem cells. *BMC Biol.* **12**, 63.
Turner, D. A., Trott, J., Hayward, P., Rué, P. and Martinez Arias, A. (2014b). An interplay between extracellular signalling and the dynamics of the exit from pluripotency drives cell fate decisions in mouse ES cells. *Biol. Open* **3**, 614-626.
Unbekandt, M. and Davies, J. A. (2010). Dissociation of embryonic kidneys followed by reaggregation allows the formation of renal tissues. *Kidney Int.* **77**, 407-416.
Vigneau, C., Polgar, K., Striker, G., Elliott, J., Hyink, D., Weber, O., Fehling, H.-J., Keller, G., Burrow, C. and Wilson, P. (2007). Mouse embryonic stem cell-derived embryoid bodies generate progenitors that integrate long term into renal proximal tubules *in vivo*. *J. Am. Soc. Nephrol.* **18**, 1709-1720.
Wilkinson, D. G., Bhatt, S. and Herrmann, B. G. (1990). Expression pattern of the mouse *T* gene and its role in mesoderm formation. *Nature* **343**, 657-659.
Wobus, A. M., Holzhausen, H., Jäkel, P. and Schöneich, J. (1984). Characterization of a pluripotent stem cell line derived from a mouse embryo. *Exp. Cell Res.* **152**, 212-219.
Wolpert, L., Tickle, C. and Martinez Arias, A. (2015). *Principles of Development*. New York: Oxford University Press.
Yallowitz, A. R., Hrycaj, S. M., Short, K. M., Smyth, I. M. and Wellik, D. M. (2011). *Hox10* Genes function in kidney development in the differentiation and integration of the cortical stroma. *PLoS ONE* **6**, e23410.
Ying, Q.-L. and Smith, A. G. (2003). Defined conditions for neural commitment and differentiation. *Methods Enzymol.* **365**, 327-341.
Zhou, J., Sharkey, J., Shukla, R., Plagge, A. and Murray, P. (2018). Assessing the effectiveness of a far-red fluorescent reporter for tracking stem cells *in vivo*. *Int. J. Mol. Sci.* **19**, 19.